BIOCHEMISTRY
including biophysical chemistry & molecular biology

ARTICLE

pubs.acs.org/biochemistry

A Biochemical Framework for SLC4A11, the Plasma Membrane Protein Defective in Corneal Dystrophies

Gonzalo L. Vilas,[†] Patricio E. Morgan,[‡] Sampath K. Loganathan,[†] Anita Quon,[†] and Joseph R. Casey*[,†]

[†]Membrane Protein Disease Research Group, Department of Physiology, and Department of Biochemistry, School of Molecular and Systems Medicine, University of Alberta, Edmonton, Canada T6G 2H7

[‡]Centro de Investigaciones Cardiovasculares, Facultad de Ciencias Médicas, Universidad Nacional de La Plata, La Plata, Buenos Aires, Argentina CP1900

Supporting Information

ABSTRACT: Mutations in the SLC4A11 protein, reported as a sodium-coupled borate transporter of the human plasma membrane, are responsible for three corneal dystrophies (CD): congenital hereditary endothelial dystrophy type 2, Harboyan syndrome, and late-onset Fuch's CD. To develop a rational basis to understand these diseases, whose point mutations are found throughout the SLC4A11 sequence, we analyzed the protein biochemically. Hydropathy analysis and an existing topology model for SLC4A1 (AE1), a bicarbonate transporter with the lowest evolutionary sequence divergence from SLC4A11, formed the basis to propose an SLC4A11 topology model. Immunofluorescence studies revealed the cytosolic orientation of N- and C-termini of SLC4A11. Limited trypsinolysis of SLC4A11 partially mapped the folding of the membrane and cytoplasmic domains of the protein. The binding of SLC4A11 to a stilbenedisulfonate inhibitor resin (SITS-Affi-Gel) was prevented by preincubation with H_2DIDS, with a significantly higher half-maximal effective concentration than AE1. We conclude that stilbenedisulfonates interact with SLC4A11 but with a lower affinity than other SLC4 proteins. Disease-causing mutants divided into two classes on the basis of the half-maximal [H_2DIDS] required for resin displacement and the fraction of protein binding H_2DIDS, likely representing mildly misfolded and grossly misfolded proteins. Disease-causing SLC4A11 mutants are retained in the endoplasmic reticulum of HEK 293 cells. This phenotype could be partially rescued in some cases by growing the cells at 30 °C.

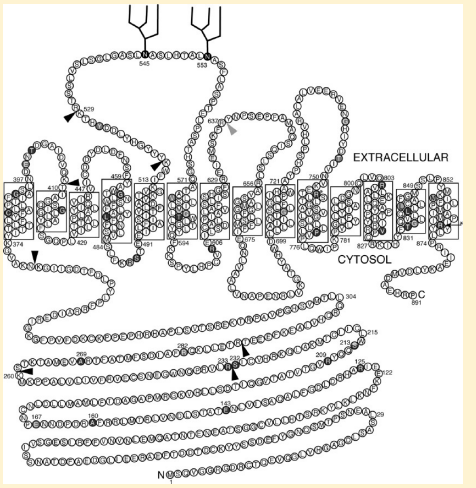

SLC4A11 was originally cloned on the basis of homology to bicarbonate transporters of the SLC4 family and was thus given the name BTR1 for (bicarbonate transporter 1).[1] SLC4A11 is an intriguing SLC4 family member because of its low degree of identity with the remaining members of the family (for example, sharing a maximum of 19% identity with SLC4A1/AE1) and its sequence similarity to the plant boron transporter BOR1.[2,3] The human *SLC4A11* gene, located at chromosome 20p12, consists of 19 exons spanning 11774 bp of genomic DNA and encodes an 891 amino acid membrane protein. Three different corneal dystrophies, congenital hereditary endothelial dystrophy type 2 (CHED2), Harboyan syndrome (HS), and some cases of Fuch's endothelial corneal dystrophy (FECD), are caused by mutations in the *SLC4A11* gene,[4−6] which has piqued interest in SLC4A11. SLC4A11-associated diseases are marked by abnormalities of the corneal endothelium and descemet membrane as well as edema of the corneal stroma.[7] In order to begin to understand the structural basis of point mutations that give rise to corneal dystrophies, we performed a biochemical characterization of SLC4A11.

The SLC4 family of plasma membrane transport proteins divides into two subfamilies on the basis of functional activity, as either electroneutral Cl^-/HCO_3^- exchangers or Na^+-coupled HCO_3^- cotransporters.[3,8,9] SLC4A11 is the only member of the SLC4 family that has not been demonstrated to transport HCO_3^-; rather, it has been reported to function as an electrogenic Na^+-coupled borate cotransporter that transports Na^+ and OH^- when boron is absent.[10] In light of this borate transport function, SLC4A11 has also been called NaBC1 for Na^+/borate cotransporter 1.[10]

SLC4A11 tissue distribution is broad, with high expression levels in the corneal endothelium, blood cells, ovary, tongue, lung, skin, and colon.[1,10] Brain, pancreas, and kidney also express SLC4A11 but to a lesser extent. Some tumors, including skin, oral, ovarian, respiratory, gastrointestinal, retinoblastoma, and leukemia, also express SLC4A11.[11] In addition to the mentioned corneal endothelial disorders CHED2, Harboyan syndrome, and FECD,[5,6,11,12] SLC4A11 defects are associated with abnormal cell growth, proliferation defects, sensorineuronal abnormalities, and polyuria.[2,10,13]

Received: November 26, 2010
Revised: February 1, 2011

There is no information available on the structure of human SLC4A11. When transiently expressed in HEK 293 cells, SLC4A11 is immunodetected as two bands of approximately 90 and 110 kDa corresponding to core and complex glycosylated forms of the protein, respectively.[6] The higher molecular mass complex glycosylated form targets to the plasma membrane, while the immature form is retained in the endoplasmic reticulum.[6] Here we studied SLC4A11 structure by characterizing N- and C-terminally epitope-tagged versions of the protein, transiently expressed in HEK 293 cells. Partial proteolytic cleavage and confocal immunofluorescence microscopy provided evidence for the topology of SLC4A11. The degree of folding of SLC4A11 and its disease alleles was assessed by the ability to bind to the immobilized inhibitor, SITS, and by sensitivity to digestion with trypsin. Finally, the ability to rescue misfolded mutant SLC4A11 from the ER was examined by growing cells expressing SLC4A11 at either 30 or 37 °C.

EXPERIMENTAL PROCEDURES

Materials. Eukaryotic expression constructs for human wild-type and mutant SLC4A11 cDNA, N-terminally tagged with the hemagglutinin (HA) epitope, were reported earlier.[5,14] SITS-Affi-Gel resin was prepared as reported previously.[15,16] Dulbecco's modified Eagle's medium (DMEM), fetal bovine serum, calf serum, penicillin−streptomycin−glutamine, and Dynabeads protein G were from Invitrogen (Carlsbad, CA, USA). Cell culture dishes were from Corning (Corning, NY, USA). Complete protease inhibitor was from Roche Applied Science (Indianapolis, IN, USA). BCA protein assay kit was from Pierce (Rockford, IL, USA). Monoclonal antibody anti-HA (clone 16B12) was from Covance (Princeton, NJ, USA). Mouse (clone 4A6) and rabbit anti-Myc antibodies were from Millipore (Billerica, MA, USA) and Abcam (Cambridge, MA, USA), respectively. IVF12 monoclonal antibody anti-AE1 was a kind gift from Dr. Michael Jennings (University of Arkansas, AR, USA). Horseradish peroxidase-conjugated donkey anti-mouse IgG was from GE Healthcare Bio-Sciences Corp. (Piscataway, NJ, USA). Alexa-coupled antibodies and Prolong Antifade Gold solution were from Molecular Probes (Carlsbad, CA, USA). Trypsin, leupeptin, and phenylmethanesulfonyl fluoride (PMSF) were from Sigma-Aldrich (Oakville, ON, Canada).

DNA Constructs. Amino- or carboxy-terminally Myc-epitope-tagged SLC4A11 (Myc-SLC4A11 or SLC4A11-Myc, respectively) chimeras were engineered by PCR using SLC4A11 cDNA in the mammalian expression vector pcDNA3.1(−) as template. Myc-SLC4A11 was constructed using the forward primer *5′-ctagctagcgccaccatggaacaaaagctaatttcagaagaagacctaagccaggtcggg-3′* that contains a 5′ *Nhe*I restriction site and introduces an N-terminal Myc-epitope tag (coding for the amino acid sequence EQKLISEEDL, underlined) to the SLC4A11 sequence removing the original initiation codon. The reverse primer *5′-agcggcgaagca-3′* hybridizes downstream of a unique *Eco*NI restriction site within the protein's coding sequence. SLC4A11-Myc was constructed in a similar way, using the forward primer *5′-gcgctctacatccaggtgat-3′* that hybridizes upstream of a unique *Bbv*CI restriction site within SLC4A11 cDNA and the reverse primer *5′-gctctagatcacaggtcttcctcactgatcagcttctgttcaggcctgtgctcagcgtc-3′* that inserts a Myc-epitope tag (EQKLISEEDL, underlined) at the C-terminal end of the SLC4A11 sequence, removing the original stop codon, and introducing a *Xba*I restriction site at the 3′ end of the amplified sequence. Clone integrity was confirmed by sequencing (DNA Core Facility, University of Alberta).

Amino Acid Sequence Analysis. Amino acid sequences for human SLC4 proteins were downloaded from pubMed (http://www.ncbi.nlm.nih.gov/pubmed). Amino acid sequences were aligned with ClustalW software (http://align.genome.jp/). Sequences corresponding to the membrane domain of each protein were defined as starting with the residue that aligned with the start of the AE1 membrane domain (V405) up to their C-terminus. Phylogenetic dendrograms for the membrane domain sequences were prepared with ClustalW software. Hydropathy plots for the amino acid sequences of full-length human AE1 and SLC4A11 were prepared with TMPred software (http://www.ch.embnet.org/software/TMPRED_form.html).

Tissue Culture. HA-SLC4A11, Myc-SLC4A11, SLC4A11-Myc, human SLC4A1 (AE1) [17], or human SLC4A1.HA [18] was expressed in HEK 293 cells by transient transfection using the calcium phosphate method.[19] Cells were grown at 37 °C (or 30 °C, where indicated) in an air/CO_2 (19:1) environment in DMEM, supplemented with 5% (v/v) fetal bovine serum, 5% (v/v) calf serum, and 1% (v/v) penicillin−streptomycin−glutamine. All experiments involving transfected cells were carried out 40−48 h posttransfection.

Immunoblot Analysis. Samples were prepared in 2× SDS−PAGE sample buffer (10% (v/v) glycerol, 2% (w/v) SDS, 0.5% (w/v) bromophenol blue, 75 mM Tris, pH 6.8), containing Complete protease inhibitor. Prior to analysis, samples were adjusted to 1% (v/v) 2-mercaptoethanol and heated for 4 min at 65 °C, and insoluble material was removed by centrifugation at 16000*g* for 10 min. Samples were then resolved by SDS−PAGE on 7.5% (w/v) acrylamide gels.[20] Proteins were electrotransferred onto Immobilon-P PVDF membranes (Millipore Corp., MA, USA). Immunoblots were prepared as previously described.[21] Membranes were then incubated for 16 h at 4 °C with gentle rocking in the presence of either mouse anti-HA, mouse anti-Myc, or IVF12 mouse anti-AE1 at 1:1500, 1:2000, and 1:3000 dilution in TBS-TM, respectively. After successive washes with TBS and TBS-T (TBS containing 0.1% (v/v) Tween-20), the membranes were incubated with a 1:5000 dilution of the appropriate HRP-conjugated secondary antibodies in TBS-TM for 1 h at room temperature and further washed with TBS and TBS-T. Proteins were detected using Western Lightning chemiluminescence reagent plus (PerkinElmer Las, Inc., MA, USA) and visualized using a Kodak Image Station 440CF (Kodak, NY, USA). Quantitative densitometric analyses were performed using Kodak Molecular Imaging Software v4.0.3 (Kodak, NY, USA).

SITS-Affi-Gel Binding Assays. HEK 293 cells were transiently transfected with cDNAs encoding HA-SLC4A11 or AE1 as described above. Forty to forty eight hours posttransfection, cells were washed with 4 °C PBS (140 mM NaCl, 3 mM KCl, 6.5 mM Na_2HPO_3, 1.5 mM KH_2PO_3, pH 7.4), lysed in IPB buffer (1% (v/v) IGEPAL CA-630, 5 mM EDTA, 150 mM NaCl, 0.5% (w/v) sodium deoxycholate, 10 mM Tris-HCl, pH 7.5), containing Complete protease inhibitor (Roche Applied Science, IN, USA), and separated into equal volume fractions. Each sample was preincubated for 1 h at 4 °C with increasing concentrations (0−500 μM) of the anion exchanger inhibitor 4,4′-diisothiocyanodihydrostilbene-2,2′-disulfonic acid (H_2DIDS). After H_2DIDS preincubation, samples were combined with 50 μL of 4-acetamido-4′-isothiocyanostilbene-2,2′-disulfonic acid slurry coupled to Affi-Gel resin (SITS-Affi-Gel resin) and further

dx.doi.org/10.1021/bi101887z |*Biochemistry* XXXX, XXX, 000–000

incubated for 15 min at 4 °C with gentle agitation.[15,16] The samples were then centrifuged for 3 min at 13200*g* at 4 °C and the supernatants recovered. As a nonspecific binding control, IPB-solubilized SLC4A11 samples were made to a final concentration of 1% (w/v) lithium dodecyl sulfate (LDS) and, after 20 min incubation on ice, subjected to the treatment described above. Samples were separated by SDS−PAGE and analyzed by immunoblotting, and the amount of HA-tagged SLC4A11 present in each aliquot was quantified by densitometry.

Partial Trypsin Digestion. HEK 293 cells were transfected with empty vector, Myc-SLC4A11, or SLC4A11-Myc. For trypsin digestion of solubilized protein, samples were lysed in 500 μL of IPB buffer in the presence or absence of protease inhibitors and immediately centrifuged at 13200*g* for 30 min at 4 °C. Supernatants were recovered and samples incubated at 0 °C with either 2 μg/mL trypsin or left untreated for 10 min. For intact cell proteolytic digestions, tissue culture dishes were washed with 4 °C PBS and incubated for 10 min at 0 °C in PBS, containing 10 μg/mL trypsin or protease inhibitors. Membrane-enriched fractions were isolated as described previously.[22] Briefly, transfected HEK 293 cells were washed in 4 °C PBS and lysed in hypotonic lysis buffer (2.5 mM $MgCl_2$, 1 mM EDTA, 1 mM dithiothreitol, 50 mM Tris-HCl, pH 8.0) in the presence or absence of protease inhibitors. Cells were passed through a 26 1/2-gauge needle 10 times and centrifuged at 400*g* for 5 min to remove nuclei and debris. The supernatant was centrifuged at 100000*g* for 30 min at 4 °C. The membrane-enriched pellet was resuspended in PBS and incubated for 10 min at 0 °C in the presence of 10 μg/mL trypsin or protease inhibitors. All trypsinolysis reactions were stopped by the addition of 1 volume of 2× SDS−PAGE sample buffer, containing 1% (v/v) 2-mercaptoethanol, 81 μM leupeptin, and 10 mM PMSF, and heating at 65 °C for 4 min. Samples were then separated by SDS−PAGE. Myc-tagged SLC4A11 was detected on immunoblots using 4A6 anti-Myc monoclonal antibody.

Confocal Microscopy. HEK 293 cells grown in 10 cm culture dishes containing 25 mm circular poly(L-lysine)-coated coverslips were individually transfected with cDNAs encoding for HA-SLC4A11, SLC4A11-Myc, AE1 bearing an HA epitope inserted at amino acid 557 in the fourth extracellular loop (SLC4A1.HA),[18] or empty vector (pcDNA 3.1 (−)). Two days post-transfection cells were washed twice with 4 °C PBS, fixed with 1% paraformaldehyde, 1 mM $CaCl_2$, and 1 mM $MgCl_2$ in PBS, pH 7.4, for 20 min at 0 °C, and washed twice with 4 °C PBS. Samples were then quenched with 50 mM NH_4Cl for 10 min at 0 °C. Fixed cells were permeabilized with 0.1% (v/v) Triton X-100 in PBS or left untreated for 1 min at 4 °C. Coverslips were then blocked for 30 min at 4 °C with 0.2% (w/v) gelatin in PBS. After blocking, samples were incubated for 1 h in a humidified chamber in the presence of 16B12 anti-HA, 4A6 anti-Myc, or IVF12 anti-AE1 [23] monoclonal antibodies at 1:1000 dilutions in 0.2% (w/v) gelatin in PBS. After three washes with 0.2% (w/v) gelatin in PBS, primary antibodies were detected by further incubation for 1 h in a dark humidified chamber in the presence of chicken anti-mouse IgG, conjugated with Alexa Fluor 488 at 1:1000 dilution in 0.2% (w/v) gelatin in PBS. Finally, coverslips were washed three times with 0.2% (w/v) gelatin in PBS, rinsed twice with PBS, and mounted in Prolong Antifade Gold solution containing the DNA-specific fluorescent dye 4′,6-diamidino-2-phenylindole (DAPI). Images were obtained with a Zeiss LSM 510 laser scanning confocal microscope (Carl Zeiss MicroImaging Inc., Germany), mounted on an Axiovert 100 M controller with a 63(NA1.4) lens.

Statistical Analysis. Values are expressed as mean ± standard error of measurement. Statistical significance analyses were performed using Prism software (Graphpad). Groups were compared with one-way ANOVA and unpaired *t*-test with $p < 0.05$ considered significant.

RESULTS

Sequence Analysis To Predict SLC4A11 Transmembrane Structure. The SLC4 family of bicarbonate transporters divides into two functional groups (subfamilies), functionally corresponding to electroneutral Cl^-/HCO_3^- exchangers (AE1, AE2, and AE3) and Na^+-coupled HCO_3^- cotransporters (SLC4A9, NBCn1, NBCn2, NDCBE, NBCe1, and NBCe2).[8] Members of these two subfamilies share a significant degree of sequence identity and therefore likely have common structural features.[8] SLC4A11 was originally included in the SLC4 family because of distant sequence similarity to electroneutral Cl^-/HCO_3^- exchangers (AE1, AE2, and AE3).[1] Phylogenetic analysis, however, indicates that SLC4A11 does not cluster strongly with either functional group but rather is placed midway between these two subfamilies, suggesting an early evolutionary divergence[8] (Supporting Information Figure 1). SLC4A11 is the most divergent of the SLC4 family (Supporting Information Figure 1). This degree of divergence raises the possibility that SLC4A11 structure is significantly different from other SLC4 members.

Electroneutral Cl^-/HCO_3^- exchangers AE1, AE2, and AE3 consist of three domains: an N-terminal cytosolic domain, a membrane domain, and a C-terminal cytosolic domain.[8] The membrane domain alone supports transport function.[24,25] Although the predicted membrane domain of SLC4A11 has only 24% sequence identity with that of AE1 (the erythrocyte membrane Cl^-/HCO_3^- exchanger, also called band 3),[3] the number and position of predicted transmembrane spans and hydropathy profiles for both proteins are strikingly similar (Supporting Information Figure 2). On the basis of the topology model for AE1 [8] and the similar hydropathy profiles that these two proteins display, we propose that SLC4A11 spans the membrane 14 times with both N- and C-termini facing the cytosol (Figure 1).

SLC4A11 has five potential consensus N-linked glycosylation sites (Asn-X-Ser/Thr) located at Asn 72, 142, 478, 545, and 553. Among these, only two localize to a potential extracellular loop (extracellular loop (EC) 3) on the topology model (Figure 1), which is the same region as AE3 but differs from AE1 where the glycosylated residue, Asn 642, is located in EC4.[8,26] We propose that SLC4A11 is glycosylated at Asn 545 or Asn 553 or both.

Orientation of N- and C-Terminal Domains. To assess the orientation of the N- and C-terminal regions of SLC4A11 relative to the plasma membrane, we used confocal microscopy. Tissue culture dishes containing HEK 293 cells grown on glass coverslips were transfected with cDNAs encoding HA-SLC4A11, SLC4A11-Myc, AE1 bearing an HA epitope tag in the fourth extracellular loop (SLC4A1.HA),[18] or empty vector. HA-SLC4A11 and SLC4A11-Myc were not detected by either anti-HA or anti-Myc antibodies when the cells were immunolabeled without cell permeabilization. HA-SLC4A11 and SLC4A11-Myc, however, were detected intracellularly and at the plasma membrane of permeabilized cells (Figure 2). In nonpermeabilized

dx.doi.org/10.1021/bi101887z |*Biochemistry* XXXX, XXX, 000–000

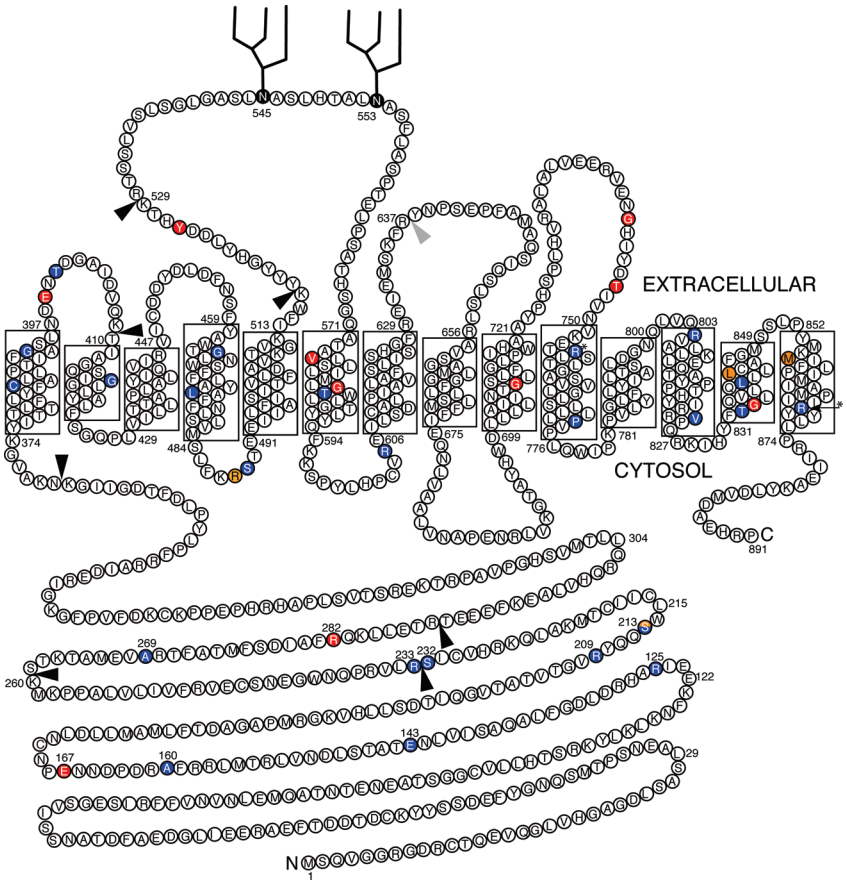

Figure 1. Topology model for human SLC4A11. Topology model for human SLC4A11 developed from the proposed structure of AE1,[26] hydrophobicity prediction algorithms (Supporting Information Figure 2), sequence alignments with AE1, immunofluorescence and proteolysis studies described in the present report. Numbers indicate amino acid position. Predicted N-glycosylation sites are in black, and the branched structures represent oligosaccharide moieties. Black and gray arrowheads indicate trypsin cleavage sites identified through partial digestion of Myc-SLC4A11 and SLC4A11-Myc, respectively. Identified point mutations causing CHED2 (blue filled), FECD (red filled), and Harboyan syndrome (orange filled) are indicated.[4−6,11,12,34,37,39,41,42] S213 was identified as mutated in both Harboyan syndrome and CHED2 and is shown in filled blue and orange accordingly. Asterisks indicate residues where two different point mutations have been found to cause disease.

cells only anti-HA antibodies were able to label the extracellular SLC4A1.HA epitope, while anti-AE1 C-terminal antibody, IVF12, produced no signal. Since the AE1 C-terminus is established as cytosolic,[27] this indicates that the fixation conditions used in this experiment do not significantly disrupt the plasma membrane integrity of the cells. SLC4A1.HA was detected in permeabilized cells with both anti-HA and IVF12. Specificity of the antibodies used is indicated by the absence of significant signal in cells transfected with empty vector (Figure 2, lower panel). Together, these results indicate a cytosolic localization of the N- and C-termini of SLC4A11, in agreement with the proposed topology model (Figure 1).

Limited Proteolysis. To probe the validity of the topology model, we examined the folded structure of SLC4A11 by limited proteolysis. Regions of the protein where cleavage sites are buried within the folded structure or transmembrane spanning segments will not be accessible to tryptic cleavage. Trypsin cleaves after Lys and Arg residues in exposed and accessible areas of a folded protein. Of the 45 Arg and 36 Lys residues in SLC4A11, 18 and 16, respectively, are within the predicted membrane domain region of SLC4A11 (from Tyr 375 to the C-terminus). Cells, transfected with N- or C-terminally Myc-tagged SLC4A11, were subjected to proteolytic digestions under a variety of conditions, including detergent-solubilized extracts, intact cells, and membrane-rich extracts (Figure 3 and Table 1). Undigested Myc-SLC4A11 and SLC4A11-Myc are found as two major bands, previously identified as representing two different glycosylation states: mature (upper) and immature (lower) protein [6] (Figure 3). Minor bands of approximately 58 and 29 kDa are also present in untreated samples from Myc-SLC4A11 and SLC4A11-Myc, respectively. These bands could arise from the action of endogenous proteases or as a result of early termination of translation. Specificity of SLC4A11 detection by the Myc epitope is revealed by the absence of immunoreactivity in lysates of vector-transfected cells. Using an average amino acid molecular mass of 110 Da and the calculated molecular mass of the tryptic fragments, we determined the length of the fragments and the corresponding nearest trypsin cleavage site on the SLC4A11 sequence (Table 1). The contribution of epitope tags to the size of each fragment was considered in assigning the positions of proteolytic sites. We did not employ mass spectrometric analysis to identify cleavage sites, as the hydrophobic peptides resulting from proteolysis of integral membrane domains do not resolve readily by mass spectrometry.[28]

Proteolytic Digestion of Intact Cells. To determine which trypsin-sensitive sites of SLC4A11 are at the exofacial side of the

dx.doi.org/10.1021/bi101887z |*Biochemistry* XXXX, XXX, 000–000

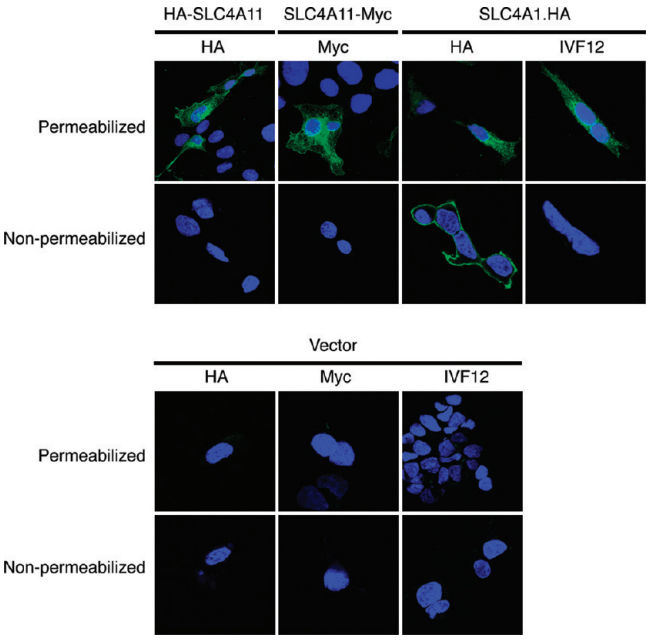

Figure 2. Localization of the N- and C- termini of SLC4A11. HEK 293 cells were transfected with cDNAs encoding HA-SLC4A11, SLC4A11-Myc, SLC4A1.HA (an AE1 construct bearing the HA epitope in the fourth extracellular loop of the protein), or empty vector. Samples were permeabilized with Triton X-100 (permeabilized) or left untreated (nonpermeabilized) and processed for confocal immunofluorescence microscopy. HA tag was detected in N-terminally tagged HA-SLC4A11 and SLC4A1.HA with monoclonal anti-HA antibody. The cytosolic C-terminal domain of SLC4A1.HA and C-terminally Myc-tagged SLC4A11-Myc were detected with IVF12 and anti-Myc monoclonal antibodies, respectively. All of the primary antibodies were detected using chicken anti-mouse IgG conjugated with Alexa Fluor 488 (green). Nuclei were detected with DAPI (blue).

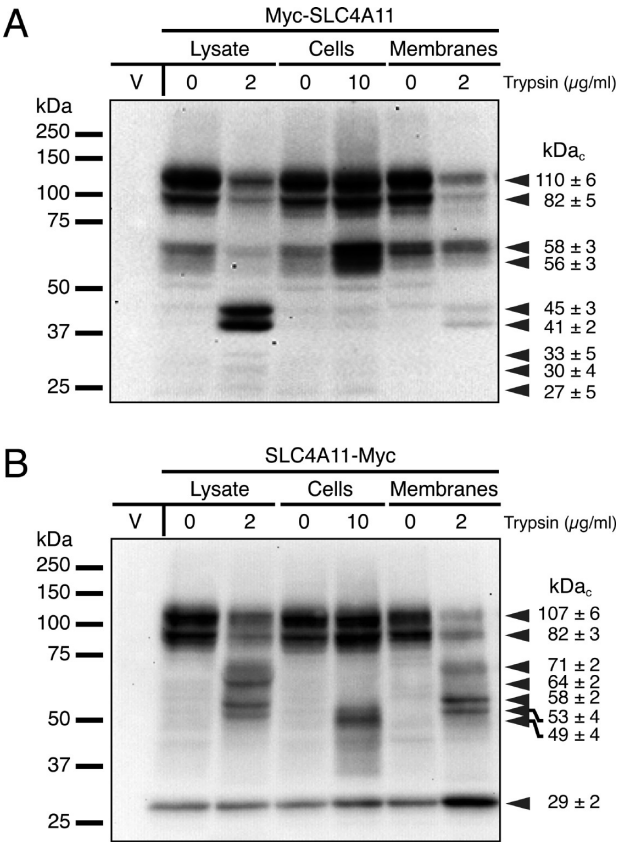

Figure 3. Partial trypsin digestion of SLC4A11. HEK 293 cells were transfected with empty vector (V) or cDNA encoding N- or C-terminally Myc-tagged SLC4A11 (Myc-SLC4A11 and SLC4A11-Myc, respectively). Samples were either solubilized in IPB (lysate), left intact (cells), or fractionated to produce a membrane-rich extract (membranes) and subjected to partial trypsin digestion. Samples were separated by SDS−PAGE and immunoblotted using anti-Myc antibody to detect Myc-SLC4A11 (A) and SLC4A11-Myc (B). Calculated molecular masses of the immunoreactive bands (kDa$_c$) were determined using the linear relationship between the relative mobility of protein standards and the logarithm of their molecular masses. Masses are presented as molecular mass ± standard error ($n \geq 3$).

plasma membrane, we treated intact HEK 293 cells, transfected with either Myc-SLC4A11 or SLC4A11-Myc cDNA, with trypsin. Immunoblots from trypsin-treated intact cells transfected with Myc-SLC4A11 revealed two major bands of 58 ± 3 and 56 ± 3 kDa and a minor band of 45 ± 3 kDa (Figure 3A, cells). These immunoreactive fragments correspond to polypeptides of 517, 499, and 399 amino acids, respectively. The nearest site that could give rise to a fragment about 399 residues long is K409, which maps well into the extracellular loop between TM 1 and TM 2 (Figure 1). Position 499 maps to the middle of a region homologous to a region accepted to be in the middle of TM 5 of AE1, while position 517 is adjacent to K516. We estimate that these fragments differ by 18 residues. We note (1) there are no Lys or Arg residues near position 319, (2) the region around 399 is almost certainly in the center of the bilayer on the basis of alignment with AE1, and (3) there is a 3 kDa (27 amino acid) error in our estimates of fragment size. We therefore assign the 58 and 56 kDa fragments to Lys 516 and Lys 529 in extracellular loop 3.

Mapping sites relative to the C-terminal Myc tag, trypsin treatment of intact cells transfected with SLC4A11-Myc generated three fragments of 53 ± 4, 49 ± 4, and 29 ± 2 kDa (Table 1, Figure 3B, cells). The 29 kDa fragment confirms the exofacial location of Arg 637 mapped in the center of EC 4. The presence of this fragment in samples that were not treated with trypsin suggests that the site is extremely sensitive to digestion and thus in a highly open conformation. Longer fragments span the site(s) of glycosylation in EC 3, meaning that they can correspond to digestion of the 110 kDa (glycosylated) or 82 kDa (unglycosylated) forms of SLC4A11. While enzymatic deglycosylation of the tryptic peptides would have clarified the identity of the fragments, it was not possible for technical reasons. Caution is thus required in interpretation of the sites of proteolysis giving rise to these fragments, since the uncertainty concerning the absence or presence of 18 kDa of glycosylation (110 kDa − 82 kDa) gives rise to 163 residue potential error. We therefore did not assign digestion positions relative to the C-terminus, except for Arg 637.

Trypsin Cleavage of Nonsolubilized Membranes. We also trypsin-treated isolated membranes of SLC4A11-expressing HEK 293 cells, in order to identify cytosolic sites in the absence of detergent. Digestion of Myc-SLC4A11 yielded a predominant fragment of 58 kDa and minor fragments of 56, 45, and 41 kDa (Figure 3, membranes, and Table 1). The 58, 56, and 45 kDa fragments were attributed above to Lys 529, Lys 516, and Lys 409, assigned to the extracellular surface of SLC4A11 (Figure 1). The 41 kDa band was not observed in digests of intact cells, suggesting that the site is intracellular. Consistent with this, the

dx.doi.org/10.1021/bi101887z |*Biochemistry* XXXX, XXX, 000–000

Table 1. Trypsin Digestion Sites Identified in SLC4A11[a]

construct	fragment mass (kDa)	estimated size of peptide (no. of residues)	corresponding position in SLC4A11	estimated site of cleavage (amino acid position)	exptl condition
Myc-SLC4A11	58 ± 3	517	517	K529*	L, C, M
	56 ± 3	499	499	K516*	L, C
	45 ± 3	399	399	K409	L, C, M
	41 ± 2	363	363	K368	L, M
	33 ± 5	291	291	R289	L
	30 ± 4	260	260	K260	L
	27 ± 5	232	232	R233	L
SLC4A11-Myc	71 ± 2	635	256		L, M
	64 ± 2	572	319		L
	58 ± 2	517	374		L, M
	53 ± 4	472	419		L, M
	49 ± 4	435	456		C
	29 ± 2	254	637	R637	L, C, M

[a] HEK 293 cells transfected with N- or C-terminally Myc-tagged SLC4A11 (Myc-SLC4A11 and SLC4A11-Myc, respectively) were either solubilized in detergent (L), left as intact cells (C), or fractionated to produce a membrane-rich extract (M) and then subjected to partial trypsin digestion. Samples were processed for immunoblotting, and the molecular masses of the immunoreactive bands were determined (see Figure 3). Fragment masses are presented as molecular mass (in kDa) ± SE ($n \geq 3$). The estimated sizes of peptides were determined from the fragment mass, assuming an average mass of 110 Da/residue, and subtracting the 10 amino acids of the Myc tag. Corresponding position in SLC4A11 is the site that would generate a fragment of the calculated estimated size. Estimated site of cleavage is the Lys or Arg residue closest to the corresponding position in SLC4A11, except for those marked with an asterisk. The Lys or Arg in the SLC4A11 sequence that would give a fragment nearest to the estimated size of peptide was identified as the estimated site of cleavage.

fragment is assigned to cleavage at Lys 368, which is just before TM 1. Since the first 368 amino acids of SLC4A11 do not contain regions of sufficient hydrophobicity to act as a transmembrane segment (Supporting Information Figure 2), the intracellular localization of Lys 368 indicates that the N-terminus to Lys 368 is cytoplasmic and constitutes a cytoplasmic domain. Digestion of SLC4A11-Myc yielded a 29 kDa fragment that confirmed accessibility of Arg 637.

Trypsin Cleavage of Whole Cell Lysates. Digestion of detergent lysates of whole cells expressing Myc-SLC4A11 gave results that were somewhat different than digests of whole membranes. The 45 and 41 kDa fragments, found as minor bands in digests of membranes, were predominant. These bands were assigned above to cleavage at Lys 409 and Lys 368, respectively (Figures 1 and 3A, lysate, and Table 1). The increased abundance of these fragments could be explained by increased proteolytic action of endogenous proteases released from organelles (i.e., lysosomes) upon detergent solubilization. Alternatively, detergent may have opened the structure of SLC4A11, resulting in increased protease accessibility. Digests of lysates confirmed fragments of 58 and 56 kDa, supporting accessibility at Lys 516 and Lys 529. Finally, faint bands at 33, 30, and 27 kDa were also observed (Figure 3A, lysate, and Table 1). We have assigned a possible cleavage site to each of these fragments. However, given the magnitude of the error on the size estimates for these fragments (36−45 amino acids) we can only conclusively say that there are three weakly accessible sites of proteolysis within the first 300 amino acids of the SLC4A11 cytoplasmic domain.

Assessment of SLC4A11 Folding Status by Limited Proteolysis. To begin to determine the nature of structural changes in SLC4A11 mutants, we performed limited proteolysis, an approach that has detected altered folding in many membrane proteins.[29,30] We prepared lysates from cells expressing WT SLC4A11 or the CHED2 mutants E143K, C386R, and R755W. In order to assess proteolytic fragments relative to the N- or C-terminus, each of these proteins was expressed as an N-terminally HA-tagged version (Supporting Information Figure 3) or C-terminally Myc-tagged version (Supporting Information Figure 4). We then examined the appearance of proteolytic fragments as a function of time of treatment with trypsin. The proteolytic patterns as assessed by the number and size of cleavage intermediates detected using anti HA antibodies were similar for WT and mutant SLC4A11 proteins (Supporting Information Figures 3 and 4). Moreover, the rate at which the full-length forms of the mutant proteins disappear was not significantly different from WT (Supporting Information Figures 3 and 4), except in the case of R755W, monitored with the C-terminal epitope tag. It was not possible to discriminate WT and CHED2 mutants of SLC4A11 on the basis of their proteolytic digestion pattern or rate of disappearance of the highest molecular mass form of protein.

Interaction of SLC4A11 with Stilbenedisulfonates. Since we could not detect changes in the structure of mutated SLC4A11 by limited proteolysis, we used an alternate approach to assess SLC4A11 folding. Stilbenedisulfonate compounds, including 4-acetamido-4′-isothiocyano-2,2′-stilbenedisulfonic acid (SITS), bind to and are classical inhibitors of SLC4 protein family members.[9,25,31] To examine possible interactions of SLC4A11 with these compounds, we examined binding to SITS immobilized on Affi-Gel resin (SITS-Affi-Gel), as described previously for AE1.[15] We also prelabeled proteins with increasing concentrations of the covalently reactive stilbenedisulfonate, H_2DIDS. Protein that does not bind to SITS-Affi-Gel thus represents the population that has its stilbenedisulfonate binding site occupied by H_2DIDS or that is incompetent to bind SITS-Affi-Gel. In this experiment the assumption is made that H_2DIDS and SITS, related stilbenedisulfonate compounds, compete for a single binding site in SLC4A11, as occurs for AE1. Since the end point of this assay is the degree of association with SITS-Affi-Gel

dx.doi.org/10.1021/bi101887z |*Biochemistry* XXXX, XXX, 000–000

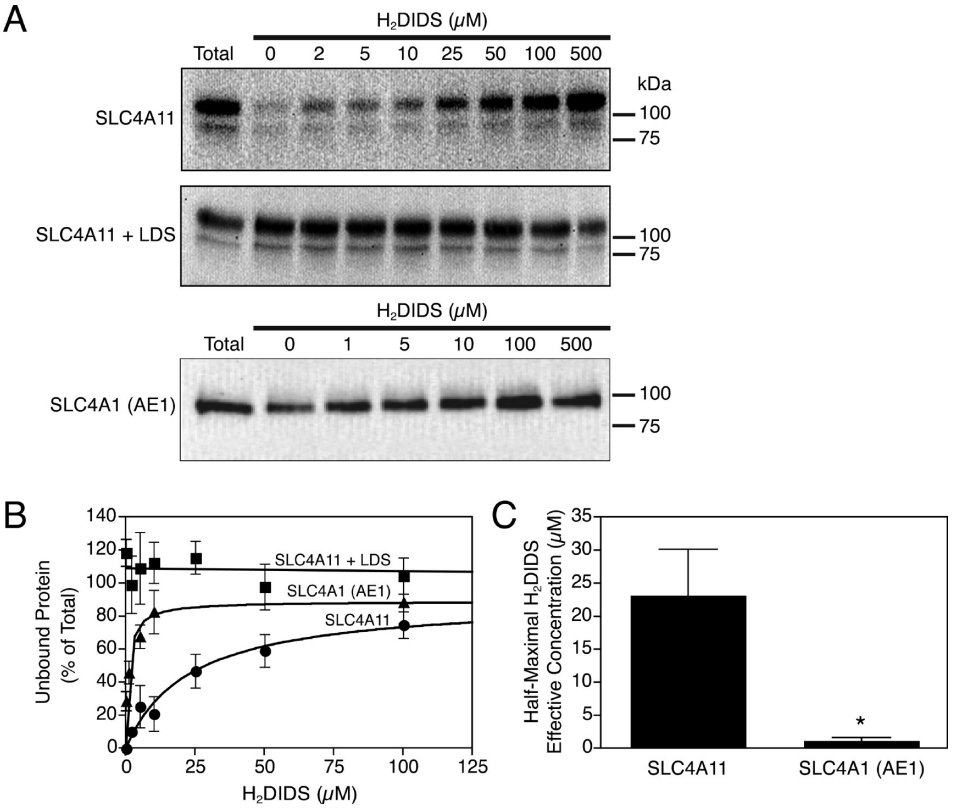

Figure 4. Interaction of SLC4A11 with immobilized inhibitor. Detergent-solubilized lysates of HEK 293 cells, transiently transfected with cDNA encoding N-terminally HA-tagged HA-SLC4A11 or AE1, were preincubated for 1 h at 4 °C with 0−500 μM anion exchanger inhibitor H_2DIDS. After H_2DIDS preincubation, samples were combined with 50 μL of SITS-Affi-Gel resin and further incubated for 15 min at 4 °C. Parallel samples were also set aside as untreated controls (total). The samples were centrifuged, and the supernatant was recovered. As a nonspecific binding control, lysates of WT SLC4A11 containing the denaturing detergent lithium dodecyl sulfate (LDS) were subjected to the same treatment. (A) SLC4A11 and AE1 were detected in the supernatant fractions on immunoblots using anti-HA and IVF12 monoclonal antibodies, respectively. (B) The amount of mature HA-SLC4A11 (upper band) or AE1 that did not bind SITS-Affi-Gel was determined by densitometry and expressed as percentage of untreated (total). (C) The H_2DIDS concentration that reduces to one-half of the protein bound to SITS-Affi-Gel resin (half-maximal effective concentration) was calculated from (B). Error bars represent standard error ($n \geq 3$). The asterisk indicates significant difference ($p < 0.05$).

resin, we cannot rule out that H_2DIDS may interact with SLC4A11 at locations outside the SITS binding site, but these events would not be detected in the SITS-Affi-Gel binding assay.

AE1, which is established to bind to stilbenedisulfonates, was immobilized by the SITS-Affi-Gel resin (Figure 4A, bottom panel). In the absence of H_2DIDS a fraction of AE1 protein did not bind the resin, which may represent misfolded protein or a limiting availability of SITS on the resin. The amount of SLC4A11 that did not bind the SITS-Affi-Gel resin increased as the H_2DIDS concentration increased (Figure 4A, upper panel). In contrast, denaturation of SLC4A11 with LDS abolished binding of the protein to the SITS-Affi-Gel resin (nearly 100% of LDS-treated SLC4A11 failed to bind SITS-Affi-Gel, Figure 4A, middle panel). This indicates that a folded conformation of SLC4A11 is required for SITS-Affi-Gel binding. Quantification of the SITS-Affi-Gel binding data (Figure 4B) revealed the interactions of the proteins with H_2DIDS and SITS-Affi-Gel. Much higher concentrations of H_2DIDS were required to prevent SLC4A11 from binding SITS-Affi-Gel than for AE1 (Figure 4C, half-maximal effective concentrations (EC_{50}) of 23 $\pm$ 7 and 1 $\pm$ 0.5 μM H_2DIDS, respectively). This indicates that SLC4A11 has a much lower affinity for H_2DIDS than does AE1. The half-maximal binding concentration observed for H_2DIDS is in line with the 0.1 and 2 μM IC_{50} values reported for the mixed and covalent interaction of DIDS with AE1, respectively.[31] Stilbenedisulfonates may be effective functional inhibitors of SLC4A11, but their effective concentration is likely 20-fold higher than found for AE1. We were unable to test whether stilbenedisulfonates affect borate transport activity of SLC4A11 as we were unable to replicate the original report of borate transport by SLC4A11 [10] (manuscript in preparation).

Discrimination of SLC4A11 Mutants Using SITS-Affi-Gel. We compared the interaction of WT HA-SLC4A11 and three CHED2 mutants (R125H, A269V, and R755W) with SITS-Affi-Gel and H_2DIDS to investigate if this assay could differentiate grossly misfolded from mildly misfolded proteins. Previously, the ability to bind stilbenedisulfonates was used to differentiate misfolded mutants of AE1 from WT AE1.[18,32,33] Under these conditions of saturating amounts of SITS-Affi-Gel, SLC4A11 mutants were fully bound to the resin, so the fraction of protein bound was unable to discriminate the protein's folded state (Figure 5A,B). The amount of mutant and WT SLC4A11 that did not bind the SITS-Affi-Gel resin increased as the H_2DIDS concentration increased (Figure 5A). Quantification of the data (Figure 5B) revealed that H_2DIDS had a half-maximal effective concentration (EC_{50}) of 19 $\pm$ 4 μM for WT HA-SLC4A11 (Figure 5C) and 29 $\pm$ 12 μM for R125H SLC4A11, which did not statistically differ from WT. EC_{50} values for A269V and

dx.doi.org/10.1021/bi101887z |*Biochemistry* XXXX, XXX, 000–000

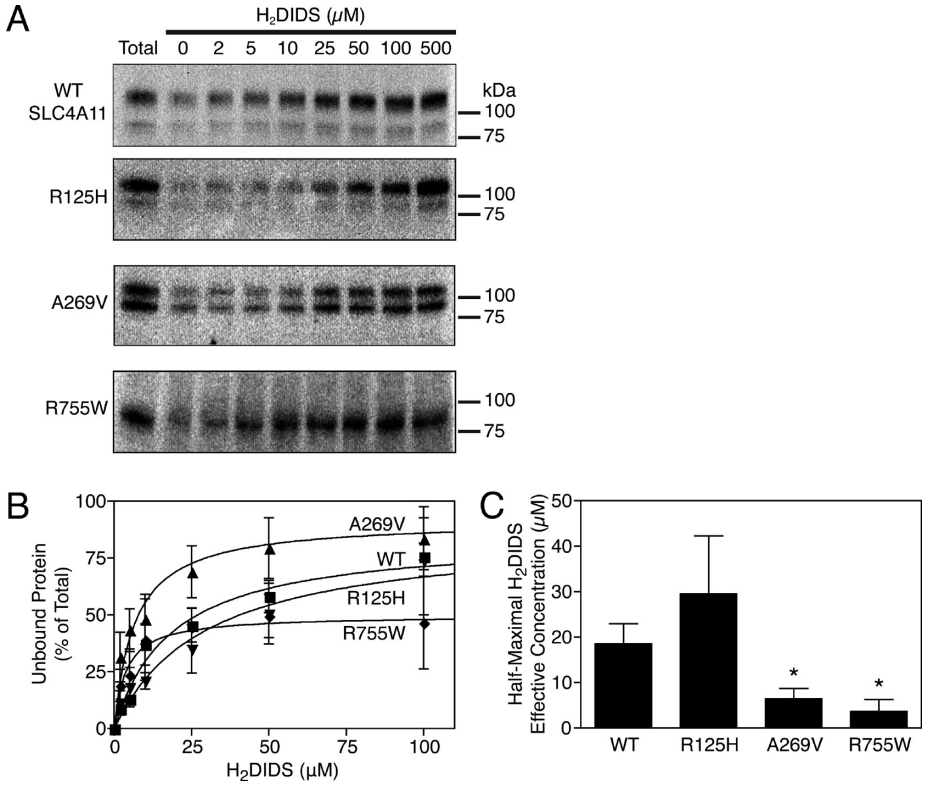

Figure 5. Binding of disease-causing SLC4A11 mutants to SITS-Affi-Gel. Lysates from HEK 293 cells, transiently transfected with cDNA encoding N-terminally HA-tagged WT or SLC4A11 disease-causing mutants, were preincubated for 1 h at 4 °C with 0−500 μM anion exchanger inhibitor 4,4′-diisothiocyanodihydrostilbene-2,2′-disulfonic acid (H_2DIDS). After H_2DIDS preincubation, samples were combined with 50 μL of SITS-Affi-Gel resin and further incubated for 15 min at 4 °C. The samples were centrifuged, and the supernatant was recovered. (A) SLC4A11 was detected in the supernatant fractions on immunoblots using anti-HA antibody. (B) The amount of SLC4A11 in each sample was determined by densitometry and expressed as a percent of the total amount of SLC4A11 incubated with the resin. (C) The H_2DIDS concentration that reduces half of the protein bound to SITS-Affi-Gel resin (half-maximal effective concentration) was calculated. Error bars represent standard error ($n \geq 3$). The asterisk indicates significant difference ($p < 0.05$) compared to mature WT SLC4A11.

R755W mutants were significantly lower (6 ± 2 and 4 ± 3 μM, respectively) compared to WT SLC4A11. Less than 50% of R755W SLC4A11 could be prevented from binding SITS-Affi-Gel by preincubation with H_2DIDS (Figure 5B). The R125H mutation appears less severe, as the mutant protein cannot be differentiated from WT SLC4A11 in the SITS-Affi-Gel binding assay. We therefore detected two changes that occur in some SLC4A11 mutants: an increase of affinity for H_2DIDS, but a fraction of protein is incompetent to interact with the compound (in the case of R755W). The assay described here can be used to assess the severity of SLC4A11 misfolding.

Rescue of Processing Defects by Low Temperature. Characterized disease-causing mutants of SLC4A11 cause retention of the protein in the endoplasmic reticulum.[5,6,34] Approaches to release ER-retained proteins to the cell surface are being investigated as a potential therapeutic, for example, as directed toward the CFTR protein that causes cystic fibrosis.[35,36] Such approaches will only be useful if the ER-retained protein is sufficiently well folded that it retains function once directed to the cell surface. The SITS-Affi-Gel approach described above presents a method to differentiate grossly misfolded mutants, which are not targets for therapeutic rescue by movement to the cell surface, from mildly misfolded mutants, which are.

To assess whether some disease-causing SLC4A11 mutants could be released from the ER and targeted to the plasma membrane, we explored the effect of low temperature cell culture on cell surface localization. WT and CHED2 mutant SLC4A11 were transfected into HEK 293 cells, and the cells were cultured at either normal 37 °C or 30 °C, the permissive temperature for many ER-retained membrane protein mutants. Maturation to the plasma membrane form was assessed by quantifying the abundance of the high molecular mass upper band of SLC4A11 (Figure 6), previously identified as corresponding to mature, plasma membrane protein.[6] In some mutants the lower band resolved into two (e.g., C386R, Figure 6A), which were previously attributed to core glycosylated (upper band) and non-glycosylated (lower band) forms, neither of which is competent for processing to the cell surface.[6] Growth at 30 °C slightly reduced the accumulation of mature WT SLC4All, possibly because protein synthesis and other cellular functions are reduced at 30 °C. The mutants divided into two classes on the basis of the effect of lowering the temperature of growth: mutants with significant increase in abundance of mature SLC4A11 (A269V, C386R) and mutants without significant increase of protein maturation (all of the other mutants studied).

DISCUSSION

Mutations in the *SLC4A11* gene have been identified in individuals with CHED2, perceptive deafness (Harboyan syndrome),

dx.doi.org/10.1021/bi101887z |*Biochemistry* XXXX, XXX, 000–000

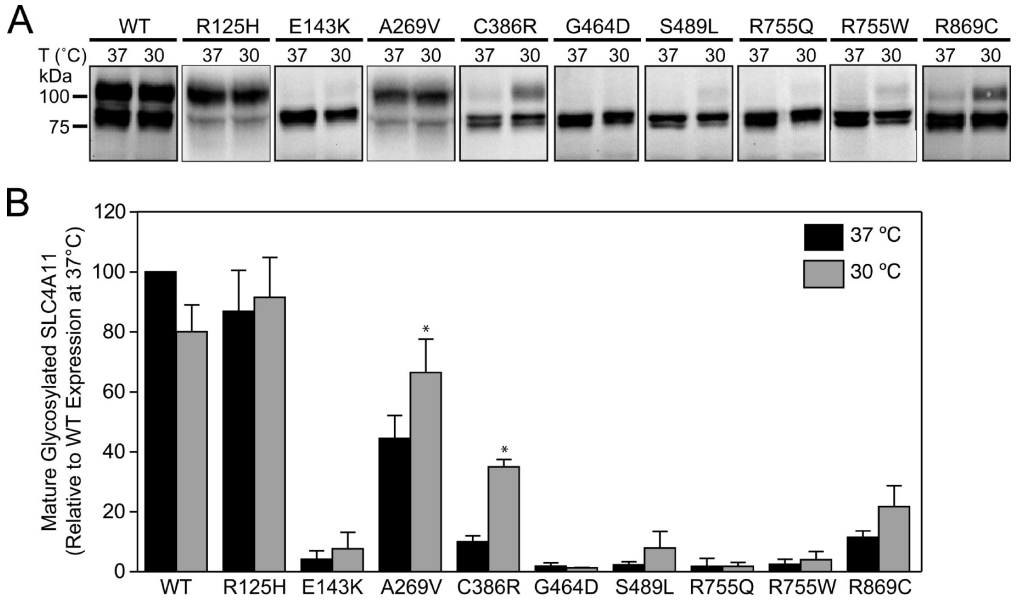

Figure 6. Rescue of SLC4A11 mutants by low temperature incubation. HEK 293 cells were transfected with cDNA corresponding to WT SLC4A11 or CHED2 mutants, as indicated. Cells were cultured for 2 days at either 30 or 37 °C, as indicated. (A) Cell lysates were subjected to immunoblotting using anti-HA monoclonal antibody. (B) The amount of the mature glycosylated, upper immunoreactive band was quantified relative to the abundance of WT SLC4A11 grown at 37 °C. Error bars represent standard error ($n \geq 3$). The asterisk indicates significant difference ($p < 0.05$) between cells grown at 37 and 30 °C.

and late-onset FECD.[5−7,12,14] Biochemical evidence is required to rationalize the identified disease-causing mutations of SLC4A11.[5,6,11,14,37−42] Hydropathy analysis, limited proteolysis, and immunofluorescent localization of epitopes provided support for a topology model for the SLC4A11 membrane domain, suggesting a fold similar to AE1. While limited proteolysis was unable to differentiate the severity of folding defects in SLC4A11 mutants, interaction of SLC4A11 with immobilized inhibitor will provide a diagnostic tool. The central defect in diseased SLC4A11 proteins is retention of the protein in the ER, preventing normal function at the cell surface. The ability to rescue SLC4A11 localization to the plasma membrane partially by cell growth at reduced temperature suggests that it may be possible to treat CHED2, FECD, and HS using pharmacological approaches.

SLC4A11 Membrane Domain Structure. This is the first study to examine the structure of SLC4A11. SLC4A11 has only 19% amino acid identity with SLC4A1 overall, or 24% in the membrane domains, so SLC4A11 is not strongly related to the other SLC4 proteins[8,9] (Supporting Information Figure 1). Thus, there is a need to ascertain SLC4A11 structure biochemically. SLC4A1 (AE1) has undergone significant biochemical analysis, allowing a detailed topology model for the protein to be developed.[26,43−46] Hydropathy analysis suggested a similar folding pattern for SLC4A11 and AE1 with three domains: a cytosolic N-terminal domain spanning residues 1−374, a membrane domain containing residues 375−873 that is organized as 14 transmembrane segments, and a short cytosolic C-terminal domain, encompassing residues 874−891. Confocal microscopy supports the cytosolic orientation of both N- and C-terminal domains proposed in the SLC4A11 topology model. Cytosolic orientation for the N-terminus to Lys 368 sequence was also supported by the absence of a cleavage site at Lys 368 except under permeabilized conditions.

In comparison to current models for AE1 two significant features have not been included in the SLC4A11 topology model (Figure 1). The first is a reentrant loop between TM 9 and TM 10,[47] which corresponds to Ala 721−Asn 750 of SLC4A11. The region between TM 9 and TM 10 is of similar size in the AE1 and SLC4A11 models (26 and 29 residues, respectively), but there is only weak sequence conservation between the proteins in this region. Second, in AE1 there is region before the last two TMs that has confusing topology on the basis of substituted cysteine accessibility experiments. The region may have an extended structure and may be conformationally dynamic.[26,46] Since there are no biochemical data to support a reentrant loop or an extended structure in SLC4A11, we have not included these elements in the current model (Figure 1).

SLC4A11 structure was further revealed by limited proteolysis. Four sites were identified as extracellular on the basis of their susceptibility to digestion in intact cells: Lys 409, Lys 516, Lys 529, and Arg 637. All of these sites are consistent with an external localization in the topology model presented as Figure 1. The SLC4A11 extracellular region has greater accessibility to trypsin digestion than AE1, since AE1 has only one external proteolytic site[48] in EC 3, a region where we identified two trypsin sites. In AE1 no trypsin site has been identified in EC1, where we found cleavage at Lys 409. We note that EC1 appears larger in models of SLC4A11 (Figure 1) than for AE1[47], and a larger loop would be more accessible to cleavage. The cleavage site at Arg 637 in EC4 corresponds to the loop that is glycosylated in AE1. In AE1 the loop is clearly aqueous accessible, since it is glycosylated and forms the Warrior blood group antigen,[49] yet no proteolytic sites have been reported there. Identification of proteolysis at Arg 637 confirms that EC4 has a sufficiently open conformation as to allow access to trypsin, aligning the structure of this region with that of AE1 EC4.

Structure of the N-Terminal Cytoplasmic Domain. The SLC4A11 N-terminal cytoplasmic domain is defined by hydropathy analysis as ending at Lys 374, while proteolytic accessibility at Lys 368 is consistent with the domain stretching at least to that

point. The role of the 374 amino acid (41 kDa) N-terminal cytoplasmic domain of SLC4A11 is unknown. While the similarly sized cytoplasmic domain of erythrocyte AE1 has well-established interactions with the cytoskeleton,[8] the cytoskeletal binding role of the AE2 and AE3 cytoplasmic domains remains unknown. The SLC4A11 cytoplasmic domain has no sequence similarity to any other protein, thus leaving the domain's function obscure. We note that in NBCe1 (SLC4A4), a sodium/bicarbonate cotransporter related to SLC4A11, the cytoplasmic domain has been proposed on the basis of molecular modeling to form a "tunnel" leading substrate to the transport site in the membrane domain.[50] Some disease-causing point mutations of the cytoplasmic domain could affect the ion channeling function and thus cause disease, but most disease alleles cause intracellular retention of the mutant protein.

Limited proteolysis does provide some insight into the structure of the cytoplasmic domain. Within the first 374 amino acids of SLC4A11 are 27 Arg and 20 Lys residues that could be trypsin sites. Like AE1 cytoplasmic domain,[51] SLC4A11 cytoplasmic domain can be cleaved readily at a site close to the membrane, consistent with an independently folding domain and an open structure as the cytoplasmic and membrane domains meet. The high abundance of the fragment arising from cleavage at Lys 368 suggests that the whole cytoplasmic domain folds as a compact structure. Three additional fragments within the cytoplasmic domain were weakly observed only in detergent lysates. These fragments, whose position could not be accurately assigned, support the notion that the domain's structure needs to be "loosened" in order to access these sites. The picture then is of a compact cytoplasmic domain with weakly accessible surface sites.

Location of Disease-Causing Mutations in the SLC4A11 Structure. The topology model presented here (Figure 1) helps to provide a structural basis for the disease alleles of SLC4A11. Many SLC4A11 disease alleles arise from profound mutations, truncation, frame-shift, or splice site mutations that can readily be seen to affect function by drastically compromising the protein.[4−6,11,12,34,37,39,41,42] Yet many disease alleles are point mutations, representing sites in the protein important either to protein function directly or whose mutations cause misfolding and ER retention. These mutations are predominantly found in the transmembrane region (Figure 1), where they are likely involved in ion permeation, or are in regions of protein−protein interaction, where mutation alters protein folding. The surprising clustering of five glycine mutations in the transmembrane region suggests that these are in positions of close protein−protein packing, where there is little tolerance for introduction of bulkier residues. Interestingly, seven mutations are in extramembraneous loops, where they may form a vestibule to conduct ions to the translocation pore. Consistent with this, in NBCe1 (SLC4A4) alterations of EC4 change ion coupling stoichiometry of the transporter.[52] Alternatively, these sites may be required to initiate transmembrane helix formation. Since FECD is a late-onset disorder, as opposed to CHED2 and Harboyan that are present at birth, FECD mutations might be considered less severe. In line with this, most of the FECD mutations are outside the plane of the lipid bilayer, where they are unlikely to be in tightly packed protein structures or to be involved in ion conduction.

Eight disease-causing point mutations map to the cytoplasmic domain (Figure 1). These cluster in the center of the domain with no reported mutations in the first 124 or last 92 amino acids of the domain. These regions may either be less important in the folding of the domain or be less important to the function of SLC4A11.

Effects of Mutations on SLC4A11 Protein. Stilbenedisulfonates inhibit the anion transport activity of SLC4 family members.[9,25,31,53] In AE1, the most studied member of the electroneutral anion exchangers, H_2DIDS covalently reacts with amino acids Lys 539 in TM 5 and Lys 851 at the end of TM 12.[54] H_2DIDS-reactive residue Lys 539 is conserved in all SLC4 family members.[25,53] In this work we show that SLC4A11 can also bind H_2DIDS with 20 times higher apparent half-maximal H_2DIDS effective concentration than AE1. In AE1 the H_2DIDS-reactive residue Lys 539 is contained in the motif KXXKIF, spanning residues 539 to 544.[26,54] Interestingly, SLC4A11 contains a similar KXXXKIF motif, spanning residues 508 to 514, that are also predicted to be at the end of TM 5. H_2DIDS is a bifunctional inhibitor, with two reactive isothiocyanate groups at each end of the molecule. In AE1, H_2DIDS covalently reacts with Lys 539 and with Lys 851 located at the end of TM 12.[54] The latter site is not conserved in SLC4A11, but we note that SLC4A11 Lys 855 localizes to the exofacial interface at TM14 in the topology model (Figure 1). While the conservation of the H_2DIDS-reactive Lys residues in SLC4A11 is interesting, we can only speculate about their involvement in stilbenedisulfonate interactions. Experiments beyond the scope of this paper will be required to fully confirm Lys 508 and Lys 855 as the H_2DIDS-reactive residues in SLC4A11. The evidence presented in this work, however, strongly suggests that this is the case.

The interaction of SLC4A11 with stilbenedisulfonates indicates that this class of compounds may be effective functional inhibitors and therefore valuable tools to characterize the functional activity of this protein. The anticipated inhibition of SLC4A11 activity by stilbenedisulfonates may prove especially useful in determining the functional role of SLC4A11 in light of our failure to replicate the report [10] that it functions as a borate transporter (submitted for publication). One previous paper found that SLC4A11 acts as a boron transporter that could not be inhibited by 500 μM DIDS.[10] The observation that H_2DIDS inhibited binding to SITS-Affi-Gel with an EC_{50} about 20 μM and the ability of SLC4A11 to bind to immobilized stilbenedisulfonate suggest that SLC4A11 transport activity will be sensitive to inhibition by stilbenedisulfonates.

Virtually all disease-causing SLC4A11 mutants are partially or completely retained intracellularly.[4−6] Intracellular-retained mutant membrane proteins may be partially functional, as seen for example in the ΔF508 allele of the cystic fibrosis gene, CFTR.[55] The rescue of retained but functional SLC4A11 mutants, for example, using small molecule folding correctors,[35] could be a viable therapeutic strategy for diseased individuals. The SITS-Affi-Gel binding assay holds the promise to differentiate grossly misfolded mutants (with capacity to bind H_2DIDS, as seen for R755W) from those with a moderate folding defect, whose interactions with H_2DIDS and SITS-Affi-Gel approximate those of WT SLC4A11 (e.g., R125H). Our results indicate that this method could be used to test the folding state of the entire set of disease-causing mutations, in order to identify those whose folding defect is possibly amenable to folding correction.

Therapeutic Implications. We used low temperature (30 °C) growth to determine whether misfolded, ER-retained SLC4A11 mutants could be released to the plasma membrane. The results were mixed, since only a fraction of SLC4A11 mutants were able to traffic to the plasma membrane. It may

be that grossly misfolded proteins cannot be released from the ER. Consistent with this interpretation, SLC4A11-R755W did not increase in its maturation when grown at 30 °C and low capacity to interact with H_2DIDS, together consistent with profound misfolding. In contrast, SLC4A11-A269V, which had WT-like interactions with H_2DIDS and SITS-Affi-Gel, showed a significant increase in protein maturation with low temperature, again suggesting that the H_2DIDS/SITS-Affi-Gel assay reflects severity of protein dysfunction and the ability for rescue. On the other hand, small molecule chemical chaperones might be more effective than low temperature in rescuing ER-retained SLC4A11 to the plasma membrane.

Do these data suggest that it might be possible to rescue SLC4A11 from the ER as a treatment for corneal dystrophies associated with SLC4A11? At maximum, SLC4A11-A269V was induced to mature to about 70% of wild-type levels. Since CHED2 is recessive, it suggests that 50% of wild-type levels of SLC4A11 suffice to prevent onset of corneal disease. If SLC4A11-A269V retains near wild-type levels of function, then maturation to 70% of WT levels should prevent disease, but it is not known how much function SLC4A11-A269V retains. There might be some hope for thermal rescue of SLC4A11 in patients. Interestingly, the cornea temperature, 34 °C,[56] is significantly lower than core body temperature, due to its location at the outer eye surface and lack of vascularization. A further reduction of 4 °C in corneal temperature, for example, with cooling eye packs during sleep, might drop corneal temperature enough to allow enough SLC4A11 maturation to limit symptom severity. More sobering is the result that only two of nine SLC4A11 mutants examined had significant increase in maturation when grown at 30 °C. Our data leave open the possibility that small molecule chaperones, administered as eye drops, could rescue the ER-retained SLC4A11.

CONCLUSIONS

We are at the early stages of discovering how defects in SLC4A11 give rise to distinct corneal dystrophies. In this report we have developed a folding model for SLC4A11, on the basis of hydropathy, sequence homology, and trypsinization, which allows disease-causing mutations to be placed in the context of membrane domain or cytoplasmic domain. Understanding the location of mutations in the context of SLC4A11 tertiary structure enables the formulation of hypotheses surrounding how mutations give rise to corneal disease. The SITS-Affi-Gel binding assay presents a method to differentiate grossly misfolded from mildly misfolded mutants of SLC4A11, identifying those that might be amenable to treatment by rescue from the ER. Supporting this, we found that a grossly misfolded mutant, identified by the SITS-Affi-Gel binding assay, could not be rescued by cell growth at 30 °C, but a mutant with a less severe folding defect was partially rescued at 30 °C. Together, this work begins to provide a framework to understand SLC4A11 disease alleles.

ASSOCIATED CONTENT

Supporting Information. Figure 1, a phylogenetic dendrogram for the amino acid sequences of the membrane domains of SLC4 proteins; Figure 2, hydropathy plots for human SLC4A1 and SLC4A11; Figures 3 and 4, data on the pattern and rate of digestion of WT and mutant SLC4A11 with trypsin, as monitored with an N-terminal (Figure 3) or a C-terminal (Figure 4) epitope tag. This material is available free of charge via the Internet at http://pubs.acs.org.

AUTHOR INFORMATION

Corresponding Author

*Phone: (780) 492-7203. Fax: (780) 492-8915. E-mail: joe.casey@ualberta.ca.

Funding Sources

G.L.V. and J.R.C. are respectively Postdoctoral Fellow and Scientist supported by the Alberta Heritage Foundation for Medical Research. P.E.M. is a Scientist supported by the Consejo Nacional de Investigaciones Científicas y Técnicas (CONICET). This work was supported by an operating grant from the Canadian Institutes of Health Research.

ACKNOWLEDGMENT

We thank Dr. Michael Jennings for providing the IVF12 monoclonal antibody and Dr. Reinhart Reithmeier for the SLC4A1.HA cDNA construct.

ABBREVIATIONS

CD, corneal dystrophy; CHED2, congenital hereditary endothelial dystrophy type 2; DAPI, 4′,6-diamidino-2-phenylindole; DIDS, 4,4′-diisothiocyanostilbene-2,2′-disulfonic acid; EC, extracellular loop; FECD, Fuch's endothelial corneal dystrophy; H_2DIDS, 4,4′-diisothiocyanodihydrostilbene-2,2′-disulfonic acid; HA, hemagglutinin; EC_{50}, half-maximal effective concentration; HEK, human embryonic kidney; HS, Harboyan syndrome; LDS, lithium dodecyl sulfate; SITS, 4-acetamido-4′-isothiocyanostilbene; TM, transmembrane segment; WT, wild type.

REFERENCES

(1) Parker, M. D., Ourmozdi, E. P., and Tanner, M. J. (2001) Human BTR1, a new bicarbonate transporter superfamily member and human AE4 from kidney. *Biochem. Biophys. Res. Commun. 282*, 1103–1109.

(2) Lopez, I. A., Rosenblatt, M. I., Kim, C., Galbraith, G. C., Jones, S. M., Kao, L., Newman, D., Liu, W., Yeh, S., Pushkin, A., Abuladze, N., and Kurtz, I. (2009) Slc4a11 gene disruption in mice: cellular targets of sensorineuronal abnormalities. *J. Biol. Chem. 284*, 26882–26896.

(3) Romero, M. F., Fulton, C. M., and Boron, W. F. (2004) The SLC4 family of HCO_3^- transporters. *Pfluegers Arch. 447*, 496–509.

(4) Desir, J., Moya, G., Reish, O., Van Regemorter, N., Deconinck, H., David, K. L., Meire, F. M., and Abramowicz, M. J. (2007) Borate transporter SLC4A11 mutations cause both Harboyan syndrome and non-syndromic corneal endothelial dystrophy. *J. Med. Genet. 44*, 322–326.

(5) Vithana, E. N., Morgan, P., Sundaresan, P., Ebenezer, N. D., Tan, , D. T., Mohamed, M. D., Anand, S., Khine, K. O., Venkataraman, D., Yong, V. H., Salto-Tellez, M., Venkatraman, A., Guo, K., Hemadevi, B., Srinivasan, M., Prajna, V., Khine, M., Casey, J. R., Inglehearn, C. F., and Aung, T. (2006) Mutations in sodium-borate cotransporter SLC4A11 cause recessive congenital hereditary endothelial dystrophy (CHED2). *Nat. Genet. 38*, 755–757.

(6) Vithana, E. N., Morgan, P. E., Ramprasad, V., Tan, D. T., Yong, V. H., Venkataraman, D., Venkatraman, A., Yam, G. H., Nagasamy, S., Law, R. W., Rajagopal, R., Pang, C. P., Kumaramanickevel, G., Casey, J. R., and Aung, T. (2008) SLC4A11 mutations in Fuchs endothelial corneal dystrophy. *Hum. Mol. Genet. 17*, 656–666.

(7) Klintworth, G. K. (2009) Corneal dystrophies. *Orphanet. J. Rare Dis. 4*, 7.

(8) Cordat, E., and Casey, J. R. (2009) Bicarbonate transport in cell physiology and disease. *Biochem. J. 417*, 423–439.

(9) Alper, S. L. (2009) Molecular physiology and genetics of Na^+-independent SLC4 anion exchangers. *J. Exp. Biol. 212*, 1672–1683.

(10) Park, M., Li, Q., Shcheynikov, N., Zeng, W., and Muallem, S. (2004) NaBC1 is a ubiquitous electrogenic Na^+-coupled borate transporter essential for cellular boron homeostasis and cell growth and proliferation. *Mol. Cell 16*, 331–341.

(11) Jiao, X., Sultana, A., Garg, P., Ramamurthy, B., Vemuganti, G. K., Gangopadhyay, N., Hejtmancik, J. F., and Kannabiran, C. (2007) Autosomal recessive corneal endothelial dystrophy (CHED2) is associated with mutations in SLC4A11. *J. Med. Genet. 44*, 64–68.

(12) Desir, J., and Abramowicz, M. (2008) Congenital hereditary endothelial dystrophy with progressive sensorineural deafness (Harboyan syndrome). *Orphanet. J. Rare Dis. 3*, 28.

(13) Groeger, N., Froehlich, H., Maier, H., Olbrich, A., Kostin, S., Braun, T., and Boettger, T. (2010) Slc4a11 prevents osmotic imbalance leading to corneal endothelial dystrophy, deafness, and polyuria. *J. Biol. Chem. 285*, 14467–14474.

(14) Hemadevi, B., Veitia, R. A., Srinivasan, M., Arunkumar, J., Prajna, N. V., Lesaffre, C., and Sundaresan, P. (2008) Identification of mutations in the SLC4A11 gene in patients with recessive congenital hereditary endothelial dystrophy. *Arch. Ophthalmol. 126*, 700–708.

(15) Pimplikar, S. W., and Reithmeier, R. A. F. (1986) Affinity chromatography of band 3, the anion transport protein of erythrocyte membranes. *J. Biol. Chem. 261*, 9770–9778.

(16) Pimplikar, S. W., and Reithmeier, R. A. F. (1988) Studies on the interaction of matrix-bound inhibitor with band 3, the anion transport protein of erythrocyte membranes. *Biochim. Biophys. Acta 942*, 253–261.

(17) Casey, J. R., Ding, Y., and Kopito, R. R. (1995) The role of cysteine residues in the erythrocyte plasma membrane anion exchange protein, AE1. *J. Biol. Chem. 270*, 8521–8527.

(18) Cordat, E., Li, J., and Reithmeier, R. A. (2003) Carboxyl-terminal truncations of human anion exchanger impair its trafficking to the plasma membrane. *Traffic 4*, 642–651.

(19) Ruetz, S., Lindsey, A. E., and Kopito, R. R. (1993) Function and biosynthesis of erythroid and nonerythroid anion exchangers. *Soc. Gen. Physiol. Ser. 48*, 193–200.

(20) Laemmli, U. K. (1970) Cleavage of structural proteins during assembly of the head of bacteriophage T4. *Nature 227*, 680–685.

(21) Basu, A., Mazor, S., and Casey, J. R. (2010) Measurement of distances within a concatamer of the plasma membrane Cl^-/HCO_3^- exchanger, AE1. *Biochemistry 49*, 9226–9240.

(22) Takida, S., and Wedegaertner, P. B. (2003) Heterotrimer formation, together with isoprenylation, is required for plasma membrane targeting of Gbetagamma. *J. Biol. Chem. 278*, 17284–17290.

(23) Jennings, M. L., Anderson, M. P., and Monaghan, R. (1986) Monoclonal antibodies against human erythrocyte band 3 protein: localization of proteolytic cleavage sites and stilbenedisulfonate-binding lysine residues. *J. Biol. Chem. 261*, 9002–9010.

(24) Grinstein, S., Ship, S., and Rothstein, A. (1978) Anion transport in relation to proteolytic dissection of band 3 protein. *Biochim. Biophys. Acta 507*, 294–304.

(25) Zhao, R., and Reithmeier, R. A. (2001) Expression and characterization of the anion transporter homologue YNL275w in *Saccharomyces cerevisiae*. *Am. J. Physiol. Cell. Physiol. 281*, C33–C45.

(26) Zhu, Q., Lee, D. W. K., and Casey, J. R. (2003) Novel topology in C-terminal region of the human plasma membrane anion exchanger, AE1. *J. Biol. Chem. 278*, 3112–3120.

(27) Lieberman, D. M., and Reithmeier, R. A. F. (1988) Localization of the carboxyl terminus of band 3 to the cytoplasmic side of the erythrocyte membrane using antibodies raised against a synthetic peptide. *J. Biol. Chem. 263*, 10022–10028.

(28) Helbig, A. O., Heck, A. J., and Slijper, M. (2010) Exploring the membrane proteome—challenges and analytical strategies. *J. Proteomics 73*, 868–878.

(29) Dorwart, M. R., Shcheynikov, N., Baker, J. M., Forman-Kay, J. D., Muallem, S., and Thomas, P. J. (2008) Congenital chloride-losing diarrhea causing mutations in the stas domain result in misfolding and mistrafficking of SLC26A3. *J. Biol. Chem. 283*, 8711–8722.

(30) Cui, L., Aleksandrov, L., Chang, X. B., Hou, Y. X., He, L., Hegedus, T., Gentzsch, M., Aleksandrov, A., Balch, W. E., and Riordan, J. R. (2007) Domain interdependence in the biosynthetic assembly of CFTR. *J. Mol. Biol. 365*, 981–994.

(31) Cabantchik, Z. I., and Greger, R. (1992) Chemical probes for anion transporters of mammalian membranes. *Am. J. Physiol. 262*, C803–C827.

(32) Kittanakom, S., Cordat, E., Akkarapatumwong, V., Yenchitsomanus, P. T., and Reithmeier, R. A. (2004) Trafficking defects of a novel autosomal recessive distal renal tubular acidosis mutant (S773P) of the human kidney anion exchanger (kAE1). *J. Biol. Chem. 279*, 40960–40971.

(33) Quilty, J. A., Cordat, E., and Reithmeier, R. A. (2002) Impaired trafficking of human kidney anion exchanger (kAE1) caused by hetero-oligomer formation with a truncated mutant associated with distal renal tubular acidosis. *Biochem. J. 13*, 895–903.

(34) Riazuddin, S. A., Vithana, E. N., Seet, L. F., Liu, Y., Al-Saif, A., Koh, L. W., Heng, Y. M., Aung, T., Meadows, D. N., Eghrari, A. O., Gottsch, J. D., and Katsanis, N. (2010) Missense mutations in the sodium borate co-transporter SLC4A11 cause late onset Fuchs corneal dystrophy. *Hum. Mutat. 31*, 1261–1268.

(35) Wang, Y., Bartlett, M. C., Loo, T. W., and Clarke, D. M. (2006) Specific rescue of cystic fibrosis transmembrane conductance regulator processing mutants using pharmacological chaperones. *Mol. Pharmacol. 70*, 297–302.

(36) Robert, R., Carlile, G. W., Liao, J., Balghi, H., Lesimple, P., Liu, N., Kus, B., Rotin, D., Wilke, M., de Jonge, H. R., Scholte, B. J., Thomas, D. Y., and Hanrahan, J. W. (2010) Correction of the delta phe508 cystic fibrosis transmembrane conductance regulator trafficking defect by the bioavailable compound glafenine. *Mol. Pharmacol. 77*, 922–930.

(37) Aldave, A. J., Yellore, V. S., Bourla, N., Momi, R. S., Khan, M. A., Salem, A. K., Rayner, S. A., Glasgow, B. J., and Kurtz, I. (2007) Autosomal recessive CHED associated with novel compound heterozygous mutations in SLC4A11. *Cornea 26*, 896–900.

(38) Desir, J., Moya, G., Reish, O., Van Regemorter, N., Deconinck, H., David, K. L., Meire, F. M., and Abramowicz, M. (2007) Borate transporter SLC4A11 mutations cause both Harboyan syndrome and non-syndromic corneal endothelial dystrophy. *J. Med. Genet. 44*, 322–326.

(39) Kumar, A., Bhattacharjee, S., Prakash, D. R., and Sadanand, C. S. (2007) Genetic analysis of two Indian families affected with congenital hereditary endothelial dystrophy: two novel mutations in SLC4A11. *Mol. Vision 13*, 39–46.

(40) Ramprasad, V. L., Ebenezer, N. D., Aung, T., Rajagopal, R., Yong, V. H., Tuft, S. J., Viswanathan, D., El-Ashry, M. F., Liskova, P., Tan, D. T., Bhattacharya, S. S., Kumaramanickavel, G., and Vithana, E. N. (2007) Novel SLC4A11 mutations in patients with recessive congenital hereditary endothelial dystrophy (CHED2). *Hum. Mutat. 28*, 522–523.

(41) Sultana, A., Garg, P., Ramamurthy, B., Vemuganti, G. K., and Kannabiran, C. (2007) Mutational spectrum of the SLC4A11 gene in autosomal recessive congenital hereditary endothelial dystrophy. *Mol. Vision 13*, 1327–1332.

(42) Aldahmesh, M., Khan, A., Meyer, B., and Alkuraya, F. (2009) Mutational spectrum of SLC4A11 in autosomal recessive CHED in Saudi Arabia. *Invest. Ophthalmol. Visual Sci. 50*, 4142–4145.

(43) Reithmeier, R. A. F., Chan, S. L., and Popov, M. (1996) Structure of the erythrocyte band 3 anion exchanger, in *Transport Processes in Eukaryotic and Prokaryotic Organisms* (Konings, W. N., Kaback, H. R., and Lolkema, J. S., Eds.) pp 281−309, Elsevier Science, Amsterdam, The Netherlands.

(44) Tang, X. B., Fujinaga, J., Kopito, R., and Casey, J. R. (1998) Topology of the region surrounding Glu681 of human AE1 protein, the erythrocyte anion exchanger. *J. Biol. Chem. 273*, 22545–22553.

(45) Tang, X.-B., Kovacs, M., Sterling, D., and Casey, J. R. (1999) Identification of residues lining the translocation pore of human AE1, plasma membrane anion exchange protein. *J. Biol. Chem. 274*, 3557–3564.

(46) Zhu, Q., and Casey, J. R. (2004) The substrate anion selectivity filter in the human erythrocyte Cl^-/HCO_3^- exchange protein, AE1. *J. Biol. Chem. 279*, 23565–23573.

(47) Cordat, E., and Casey, J. R. (2009) Bicarbonate transport in cell physiology and disease. *Biochem. J. 417*, 423–439.

(48) Jennings, M. L., and Passow, H. (1979) Anion transport across the erythrocyte membrane *in situ* proteoysis of band 3 protein, and cross-linking of proteolytic fragments by 4,4′-diisothiocyanodihydrostilbene-2,2′-disulfonate. *Biochim. Biophys. Acta 554*, 498–519.

(49) Jarolim, P., Murray, J. L., Rubin, H. L., Coghlan, G., and Zelinski, T. (1997) A Thr552 → Ile substitution in erythroid band 3 gives rise to the Warrior blood group antigen. *Transfusion 37*, 398–405.

(50) Chang, M. H., Dipiero, J., Sonnichsen, F. D., and Romero, M. F. (2008) Entry to "HCO_3^- tunnel" revealed by SLC4A4 human mutation and structural model. *J. Biol. Chem. 283*, 18402–18410.

(51) Wang, D. N. (1994) Band 3 protein: structure, flexibility and function. *FEBS Lett. 346*, 26–31.

(52) Chen, L. M., Liu, Y., and Boron, W. F. (2011) Role of an extracellular loop in determining the stoichiometry of Na/HCO3 cotransporters. *J. Physiol.*, published online before print January 4, 2011, doi: 10.1113/jphysiol.2010.19873.

(53) Pushkin, A., and Kurtz, I. (2006) SLC4 base (HCO_3^-, CO_3^{2-}) transporters: classification, function, structure, genetic diseases, and knockout models. *Am. J. Physiol. Renal Physiol. 290*, F580–F599.

(54) Okubo, K., Kang, D., Hamasaki, N., and Jennings, M. L. (1994) Red blood cell band 3. Lysine 539 and lysine 851 react with the same H_2DIDS (4,4′-diisothiocyanodihydrostilbene-2,2′-disulfonic acid) molecule *J. Biol. Chem. 269*, 1918–1926.

(55) Cormet-Boyaka, E., Jablonsky, M., Naren, A. P., Jackson, P. L., Muccio, D. D., and Kirk, K. L. (2004) Rescuing cystic fibrosis transmembrane conductance regulator (CFTR)-processing mutants by transcomplementation. *Proc. Natl. Acad. Sci. U.S.A. 101*, 8221–8226.

(56) Tan, L., Cai, Z. Q., and Lai, N. S. (2009) Accuracy and sensitivity of the dynamic ocular thermography and inter-subjects ocular surface temperature (OST) in Chinese young adults. *Contact Lens Anterior Eye 32*, 78–83.